聚（醯胺-亞醯胺）/氧化石墨烯奈米複合薄膜具水氣阻隔特性之研究

Poly(amide-imide)/graphene oxide nanocomposite films with improved moisture barrier property

葉珮綺 [1]、張謹文 [1]、曾怡享 [2]、蔡美慧 [1]*
PEI-CI YE [1], Chin-Wen Chang[1], Mei-Hui Tsai [1]*, I-Hsiang Tseng[2]

[1] 國立勤益科技大學化工與材料工程系
[1] Department of Chemical and Materials Engineering,
National Chin-Yi University of Technology
E-mail：tsaimh@ncut.edu.tw
[2] 逢甲大學化學工程系
[2] Feng Chia University
Department of Chemical Engineering
E-mail：ihtseng@fcu.edu.tw

摘要

以不同重量百分比的氧化石墨烯(Graphene Oxide, GO)透過溶液分散法分散在聚亞醯胺(Polyimide；PI)及聚(醯胺-亞醯胺) (Poly(amide-imide)； PAI)前驅物中，接著藉由亞醯胺化製備出二種不同的複合薄膜(PI/GO、PAI/GO)。在本實驗中加入trimellitic anhydride chloride (TMAC)至PAI/GO中，PAI中的醯胺基會與GO的羧酸基、羥基等官能基產生作用力，最後再進行PI/GO和PAI/GO的阻水及其他特性之探討。

關鍵字詞：聚亞醯胺; 聚(醯胺-亞醯胺); 氧化石墨烯; 水氣穿透速率(WVTR)

Abstract

Different weight amounts of graphene oxide (GO) were solution-dispersed with the precursor of polyimide (PI) and poly(amide-imide) (PAI) to synthesizen PI/GO or PAI/GO composite films after the imidization process. The addition of trimellitic anhydride chloride (TMAC) in PAI/GO matirx provides the interaction between amide group on PAI and carboxy/hydroxyl groups on GO.The effects of TMAC and GO amounts on the water barrier and other properties of PI/GO and PAI/GO were investigated in this study.

Keywords: polyimide; poly(amide-imide); grapheneoxide;; water-vapor-transmission-rate (WVTR)

1. Introduction

Aromatic polyimides(PIs) are one of the most useful classes of high performance polymers [1]. These materials exhibit high electrical resistivity, excellent mechanical and thermal properties that they are widely used in semiconductors, optoelectronics and microelectronics industries. However, severe drawback of PIs is their high

water/oxygen permeation, which limits the performance or service life of those electronics using PIs as substrates [2,3].

Recently, layered graphene has attracted tremendous attention, because of its extraordinary electronic and mechanical properties. In addition, graphene and graphene-derived layered materials are also good barrier propertie as potential candidates of water/oxygen barrier membranes, due to graphene have very large surface areas. Poly(vinyl alcohol) and graphene oxide (GO) nanocomposites are shown to reduce oxygen transmission [3-7]. Previously, we developed to synthesize colorless PI/GO nanocomposite films, in order to improve the water barrier property of PI films. PI/GO nanocomposite films resulted in an 90% lower WVTR. [3]. However, weak interfacial interactions between the GO and the PI matrix, thus limit the dispersion of GO nanofiller materials in PI [8]. Modification of PI imparts improved GO compatibility, reinforcing GO in PI composites. Copolycondensation is one of the possible structural modifications of polymer properties. Modification of the properties of PIs by incorporation of hydrogen-bonded amide groups has been deserved particular attention and poly(amide-imide)s (PAIs) have been studied extensively. PAIs combines the high thermal stability of PIs and ease of processability of polyamides [1, 9-11].

In this study, GO can be produced from inexpensive graphite powder by Hummers method and followed by exfoliation [12,13]. This heavily oxygenated compounds bear hydroxyl and epoxide functional groups on their basal planes with carbonyl and carboxyl groups located at the sheet edges [14-17]. The addition of trimellitic anhydride chloride (TMAC) in PAI/GO matirx provides the interfacial hydrogen bonding interactions between amide group on the PAI backbone and carboxyl /hydroxyl groups on GO. The objective of this study is to evaluate the effects of TMAC and GO content on the water-vapor-transmission-rate (WVTR). The results suggest that PAI/GO reduce the moisture permeation than PI/GO, because of PAI have more compatibility with GO than PI. In addition, the obtained PAI/GO nanocomposites exhibit excellent high temperature dimensional stability and mechanical strength.

2.Experimental

2.1 Materials

3,3',4,4'-benzophenetetracarboxylic anhydride （BTDA) and 4,4'-diaminodiphenylether (ODA) were provided by Taimide Tech Inc. (Taiwan). Trimellitic Anhydride Chloride （TMAC） was purchased from Alfa Aesar. N-methyl-2-pyrrolidinone（NMP）were provided by TEDIA. Potassium permanganate ($KMnO_4$), sodium nitrate ($NaNO_3$), hydrogen peroxide (H_2O_2), and sulfuric acid (H_2SO_4) were commercially obtained from Showa Chemical Co. Graphite powder (325 mesh) was supplied by Alfa-Aesar.

2.2 Preparation of graphene oxide (GO)

GO was exfoliated from graphite by the following modified Hummers method [14-15, 20]. 5 g of natural graphite and 2.5 g of $NaNO_3$ were stirred with 115 mL of H_2SO_4 (98%) in a 250 mL three-neck flask in an ice bath, and followed by the slow addition of 15g of $KMnO_4$. In the subsequent three hours, the ice bath was removed and being heated to 35±3 ℃ for 30 min. At the end of 30 minutes, 230 mL of deionized water was slowly poured into a flask and further heated to temperature to 98℃.After holding the temperature

constant for 15 min, the mixture was then poured into 1 L of warm deionized water. The residual potassium permanganate and manganese dioxide were removed by the addition 35 mL of H_2O_2. The GO obtained was then purified by repeated centrifugation and redispersing in deionized water until a pH value of 6. The GO powder was obtained after drying at 60 °C for 24 h in a vacuum oven.

2.3 Preparation of PI/GO and PAI/GO nanocomposite films

The synthesize procedure of PI/GO or PAI/GO films was shown in Scheme. 1. The PI/GO or PAI/GO films was made by reacting stoichiometrical amount of ODA, TMAC, BTDA (molar ratio of ODA: TMAC: BTDA was shown in Table. 1.) and suitable amount of NMP under a nitrogen atmosphere and mechanical stirring for 3 h. Suitable stoichiometric ratio of ODA and NMP was added in a three-necked flask equipped and stirred at room temperature. After thoroughly stirred and dissolved, TMAC was added in sequence. Half of BTDA was sequentially mixed with above solution to obtain a poly(amic acid) or poly(amide amic acid) solutions (PAA) solution. Various amounts of GO were dispersed in NMP with the assistance of ultrasonic vibration prior to mixing with the PAA. The final portion of BTDA was mixed and continuously stirred at room temperature for 3 h to obtain homogeneous viscous PAA/GO solution. The PAA/GO was cast on a glass plate, and 250 μm thick films obtained by knife coating and then cured in an air-circulating oven at 80, 100, 150 and 200 °C for annealing at each 1 h and finally to 350 °C and annealing for 2 h. The nanocomposite films had an average final thickness of 25-30 μm. The sample code were denoted PI-y-TMAC/x, where y represents the molar ratio of TMAC, x represents the wt% of GO in PI nanocomposites. In this study, x was ranging from 0.5 to 20.

2.4 Measurements

The morphology of GO, PI and PAI nanocomposites were investigated using transmission electron microscopy (TEM; Hitachi H-7100) & (TEM; Tecnai G2, 200kV, high resolution). The samples were prepared by drying a droplet of the suspension on 400-mesh carbon-coated copper grids. X-ray diffraction (XRD) experiments were conducted on an X-ray diffractometer (PANalytical X'Pert PRO) using Cu Kα radiation (λ= 0.154 nm) at an accelerating voltage of 40 kV and current of 30 mA to study the crystalline structure of the nanofillers used in the study. Fourier transform infrared (FTIR) spectra of PI, PAI, PI/GO and PAI/GO nanocomposites were recorded between 4000 and 400 cm^{-1} by Nicolet PROTEGE-460 FTIR spectrophotometer equipped. The dynamic mechanical analysis (DMA, TA 2980) was performed at a frequency of 1 Hz, from 60 ℃to 350℃ and at a heating rate of 3℃/min. The in-plane coefficient of thermal expansion (CTE) of samples was determined from TMA measurements (TA Q400), with a tension force of 0.05 N, at a heating rate of 10°C/min, at a frequency of 1 Hz and under nitrogen. The water vapor transmission rate (WVTR) of samples with the size of 10 cm^2 was measured using a Permatran-w3/61 model system at atmospheric pressure, 40 °C and 100% relative humidity.

3. Results and discussion

3.1 Characteristics of GO

The morphology and XRD pattern of obtained

GO were shown in Fig. 1. The TEM image of GO sheet was shown in Fig. 1(a) Most parts of the sheets tend to fold and wrinkled. We also observed lattice fringes structure of carbons in some regions, especially the edges or the folding of the GO nanosheets, from the HR-TEM image was shown in Fig. 1(b). The separation between neighboring fringes was measured as ~0.68 nm and was larger than the interplanar spacing in graphite (0.34 nm), because of the presence of oxygen functional groups on the GO layers as well as the possible inclusion of interlamellar molecules [7,21]. The XRD pattern shown in Fig. 1(c). revealed the characteristic intense refraction peak of graphite at $2\theta = 26.4^{o}$, which corresponds to the graphene interlayer of (002) with the d-spacing of 0.34 nm [3,8,22]. After oxidation by Hummers method, GO had a weak diffraction peak at $2\theta = 10.0^{o}$ and the d-spacing of the neighboring layers were ~ 0.88 nm indicated the intercalation by oxygen groups and moisture. As well as the shift to lower angle, peak broadening took place because of the disorder introduced by reduced average crystalline size [3,4].

3.2 FTIR of PI/GO and PAI/GO anocomposites

The FTIR spectra of pure PI, PI-0.5-TMAC, PI-1-TMAC and PI-1-TMAC/10 films were shown in Fig. 2. The characteristic imide absorption bands at 1380 cm^{-1} (C-N stretching), 1700 cm^{-1} and 1780 cm^{-1} (symmetrical and asymmetrical C=O stretching) were observed on the IR spectra of PI and PAI hybrid films. Meanwhile, the peak at 3375 and 3065 cm^{-1} corresponding to N-H bending in PI-0.5-TMAC shifted to 3367 and 3050 cm^{-1} in PI-1-TMAC ; the peaks at 1647 cm^{-1} corresponding to C=O bending in PI-0.5-TMAC shifted to 1645 cm^{-1} in PI-1-TMAC. It shows that larger absorption intensity and shifts to lower frequency. The result could be evidenced that the intermolecular hydrogen bonding of PI films were increased as the increase of TMAC content [23] By comparing PI-1-TMAC with PI-1-TMAC/10, it was seen that the presence of GO shifts some peaks to lower wavenumbers. For instance, the peaks of N–H and C=O bending in PI-1-TMAC were at 3367, 3050 cm^{-1} and 1645 cm^{-1}, respectively; while those for the PI-1-TMAC/10 shifted to 3355, 3049 cm^{-1} and 1642 cm^{-1} respectively. These results also implied the presence of a strong hydrogen-bonding interaction between GO and PAI [24]

3.3 Dispersion of PI/GO and PAI/GO anocomposites

The TEM micrographs of PI/10, PI-0.5-TMAC/10 and PI-1-TMAC/10 nanocomposites were shown in Fig. 3. It could be also observed that the dispersion extent of PI-1-TMAC/10 nanocomposites was apparently better than PI-0.5-TMAC/10 nanocomposites and the dispersion extent of PI-0.5-TMAC/10 nanocomposites was apparently better than PI/10 nanocomposites. As for the results, the reason should be ascribed to increase of TMAC content will enhance the intermolecular attraction of GO.

3.4. Mechanical and Thermal properties of PI/GO and PAI/GO nanocomposites

The storage modulus (E′), glass transition temperature (Tg) and damping (Tan δ) of the PI/GO and PAI/GO nanocomposites were determined by DMA and the results were shown in Table 2. The storage modulus (E′) of hybrid films increased remarkably with the increase of GO contents. The series of PI-1-TMAC/GO hybrid films was obviously better than PI-0.5-TMAC/GO and PI/GO hybrid films. The (E′) value at 60 ℃ was 2151 MPa

for PI-1-TMAC and increased to 3441 MPa for PI-1-TMAC/10. The reinforcement effect from GO was mainly attributed to its fine dispersion and high orientation in PAI matrix, as well as the efficient load transfer from the matrix to GO nanosheets, and thus significantly enhanced the mechanical strength of nanocomposites. The temperature at the maximum of Tan δ curve was designated as the glass transition temperature (Tg). The negligible variation in Tg values with GO content. The peak intensity of Tan δ (damping value) decreased as increase of TMAC and GO content. The Tan δ value was 1.23 for PI and 0.92 for PI /10; 1.06 for PI-0.5-TMAC and 0.69 for PI-0.5-TMAC/10; 0.26 for PI-1-TMAC and 0.20 for PI-1-TMAC/10 nanocomposites. A very large value of Tan δ (<<1) indicated liquid-like materials and a very small value (>>1) indicates solid-like materials. Moreover, the damping value of hybrid films was an indicator to determine weakly associated (Tan δ < 1) or strongly associated (Tan δ > 1) dispersed particles in nanocomposites [25]. Therefore, the synthesized PI/GO and PAI/GO nanocomposites with higher GO content became more solid-like as well as the dispersed GO particles became more strongly.

The coefficient of thermal expansion (CTE) of the PI/GO and PAI/GO nanocomposites from the TMA between 100 and 200 ℃ were investigated as listed in Table 2. The CTE of the PI/GO and PAI/GO nanocomposites decreased as the GO content increases. The reason was that one-dimensional GO nanosheets could be enhance the chain orientation of PI and thus resulting to lower CTE [8].

3.5. Moisture barrier of PI/GO and PAI/GO nanocomposites

The WVTRs of PI/GO and PAI/GO nanocomposites were shown in Fig. 4. The WVTR of series of PI-1-TMAC/GO films were the lowest one compared with series of PI-0.5-TMAC/GO and PI/GO films, respectively. A significant decrease in WVTR by 92%, from 130.03 to 10.27 g-m/m^2-day, was observed upon the addition of 10 wt% of GO in PI-1-TMAC matrix. The the strong interfacial adhesion between GO and PI-1-TMAC matrix, distribution of GO with the features of high aspect ratio and high specific surface area in PI-1-TMAC matrix could effectively extend the path of the water vapor passing through the thin film [8], thus significantly improved water vapor barrier property.

4. Conclusions

In this study, we had successfully incorporation of GO nanosheets in PAI, the resultant PAI/GO nanocomposites had enhanced mechanical strength and dimensional stability. The storage modulus increased and damping intensity decreased as the increase of TMAC and GO content. Most importantly, the PI-1-TMAC/10 nanocomposite significant decrease in WVTR by 92% and exhibited the lowest moisture transmission rate, 10.27 g-m/m^2-day. The results suggested the synthesized PAI/GO nanocomposites were potential candidates for the applications, such as the substrates of advanced flexible display, where good water resistance was essentially required.

Table 1. Mole ratio of PI and PAI.

Sample code	ODA	BTDA	TMAC
PI	1	1	0
PI-0.5-TMAC	1	0.5	0.5
PI-1-TMAC	1	0	1

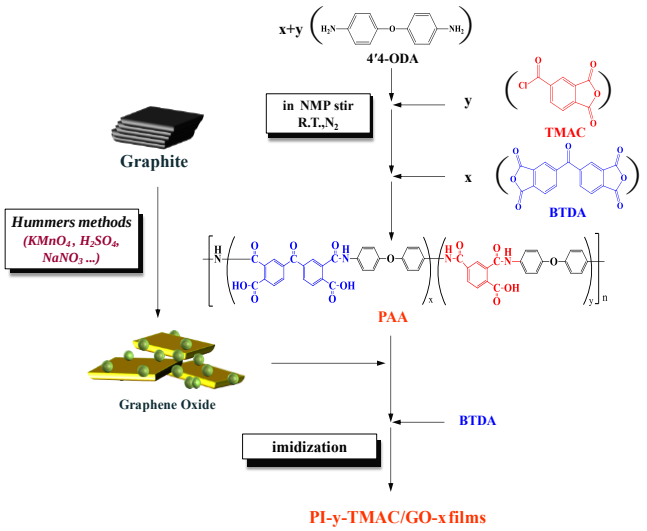

Scheme. 1. Preparetion of chemical structure of PI-y-TMAC films.

Table 2. Mechanical and thermal properties of pure PI ,PAI, PI/GO and PAI/GO films.

Sample code	DMA			TMA
	E′ [a] (MPa)	Tg (℃)	Tan δ	CTE [b] (ppm/℃)
PI	1557	295	1.23	59.9
PI/0.5	1565	296	1.10	57.3
PI/1	1749	295	1.09	55.9
PI/5	1905	292	1.06	51.3
PI/10	2607	294	0.92	52.4
PI-0.5-TMAC	1952	298	1.06	56.4
PI-0.5-TMAC/0.5	2139	296	1.03	55.0
PI-0.5-TMAC/1	2134	296	1.02	54.7
PI-0.5-TMAC/5	2663	290	0.91	51.0
PI-0.5-TMAC/10	2938	293	0.69	47.1
PI-1-TMAC	2151	305	0.26	57.7
PI-1-TMAC/0.5	2163	297	0.26	55.1
PI-1-TMAC/1	2963	304	0.20	57.7
PI-1-TMAC/5	3223	300	0.20	49.7
PI-1-TMAC/10	3441	303	0.20	48.1

[a] Determined from the DMA results in the temperature of 60℃.
[b] Determined from the TMA results in the temperature of 100-200 ℃.

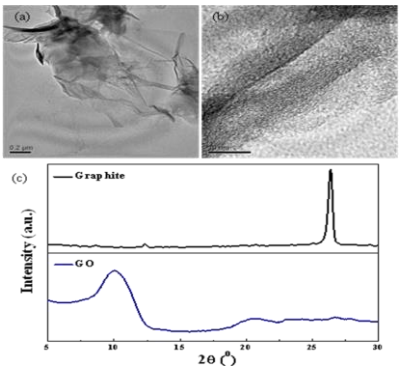

Fig. 1 (a) TEM images of a multilayer GO sheet and (b) The HRTEM image shows the folded edge of the bare GO sheet. ; (c) XRD patterns of graphite and dried GO.

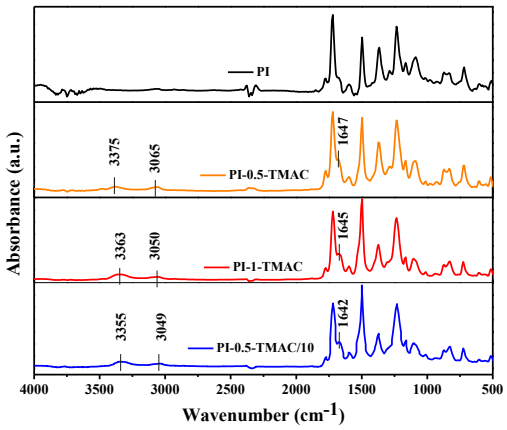

Fig. 2 FTIR spectra of pure PI, PI-0.5-TMAC, PI-1-TMAC and PI-1-TMAC/10 films.

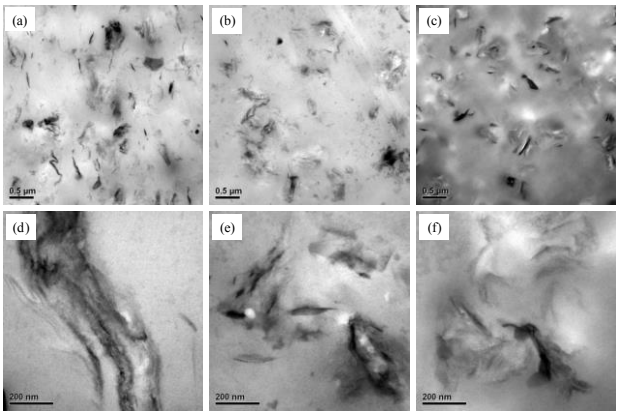

Fig. 3. TEM image of (a)(d) PI/10 at magnification 20K × (b)(e) PI-0.5-TMAC/10 at magnification 20K ×, (c)(f) PI-1-TMAC/10 filmsat magnification 20K ×, (d) PI/10 at magnification 100K ×, (e) PI-0.5-TMAC/10 at magnification 100K ×, (f) PI-1-TMAC/10 filmsat magnification 100K ×.

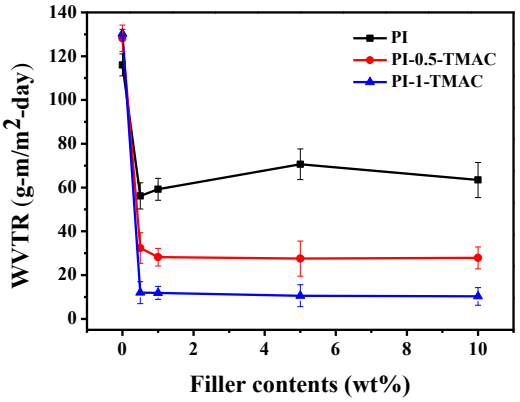

Fig. 4. Effect of GO contents on the water-vapor-transmission-rate (WVTR) of PI/GO and PAI/GO nanocomposite films. Note: WVTR was measured at 40 ℃ and 100% RH.

5. References

[1] G. Eda, M. Chhowalla, Adv. Mater. 22 (2010) 2392-2415.

[2] D. Zheng, G. Tang, H.-B. Zhang, Z. Z. Yu, F. Yavari, N. Koratkar, S. H. Lim,
M.W. Lee, Composites Science and Technology. 72 (2012) 284-289.

[3] H. Kim, Y. Miura, C. W. Macosko, Chem. Mater. 22 (2010) 3441-3450.

[4] H. M. Kim, J. K. Lee, H. S. Lee, Thin Solid Films.519 (2011) 7766-7771.

[5] L. Yu,Y. S. Lim, J. H. Han, K. Kim, J. Y. Kim, S. Y. Choi, K.W. Shin,Synthetic Metals. 162 (2012) 710-714.

[6] I. H. Tseng, C. J. Chang , C. W. Chang , H. H. Lu , M. H. Tsai, Surface & Coatings Technology. (2012).

[7] I. H. Tseng, Y. F. Liao, J. C. Chiang, M. H. Tsai, Society of Chemical Industry. (2012).

[8] I. H. Tseng, Y. F. Liao, J. C. Chiang, M. H. Tsai, Materials Chemistry and Physics. 136 (2012) 247-253.

[9] J. Y. Wang, S. Y. Yang, Y. Li. Huang, H. W. Tien, W. K. Chin, C.C. M. Ma, J. Mater. Chem. 21 (2011) 13569-13575.

[10] P. Thiruvasagam, M. Vijayan, Journal *of* Polymer Research. 19 (2012) 1-9.

[11] E. A. Lotf, A. Shockravi, Polymer Degradation and Stability. 96 (2011) 1022-1028.

[12] Z. Sonia, A. Zahoor, Colloid Polym Sci. 285 (2007) 1749-1754.

[13] M. L. Moslem, M. Masoud , J Polym Res. 16 (2009) 681-686.

[14] W.S. Hummers Jr., R.E. Offeman, J. Am. Chem. Soc. 80 (1958) 1339.

[15] H. L. Poh, F.Sanek, A. Ambrosi, G. Zhao, Z. Sofer, M. Pumera, Nanoscale. 4 (2012) 3515-3522.

[16] H. He, J. Klinowski, M. Forster, A. Lerf, Chem. Phys. Lett. 287 (1998) 53-56.

[17] A. Lerf, H. He, M. Forster, J. Klinowski, J.Phys.Chem. B. 102 (1998) 4477-4482.

[18] G. Y. Kim, M. C. Choi, D. Lee, C. S. Ha, Macromol. Mater. Eng. 297 (2012) 303-311.

[19] H. D. Huang , P. G. Ren, J. Chen , W. Q. Zhang ,Journal of Membrane Science. 409-410 (2012) 156-163.

[20] I. H. Tseng, J. C. Chang, M. H. Tsai, Polymer International. (2012).

[21] G. Lu, S. Mao, S. J. Park, R. S. Ruoff, J. H. Chen, Nano Res. 2 (2009) 192-200.

[22] B. H. Kim, J. H. Jung, S. H. Hong, J. Joo, Macromolecules. 35 (2002) 1419-1423.

[23]M. H. Tsai, S. L. Huang, J. C. Muti Lin, C. J. Ko, Y. L. Chen, C. M. Lu, C. J. Chen,C. H. Yen, Journal of Applied Polymer Science. 105 (2007) 3689-3697.

[24]R. Q. Liu, S. M. Liang, X. Z. Tang, D. Yan,J. Mater. Chem. 22 (2012) 14160-14167.

[25] M. H. Tsai, Y. C. Huang, I. H. Tseng, Thin Solid Films. 519 (2011) 5238-5242.